Dalton Transactions

Accepted Manuscript

ROYAL SOCIETY OF CHEMISTRY

www.rsc.org/dalton

Bond ionicity, lattice energy, bond energy and microwave dielectric properties of $ZnZr(Nb_{1-x}A_x)_2O_8$ (A=Ta, Sb) ceramics

Ping Zhang[a]*, Yonggui Zhao[a], Haitao, Wu[b]

[a]*School of Electronic and Information Engineering and Key Laboratory of Advanced Ceramics and Machining Technology of Ministry of Education, Tianjin University, Tianjin 300072, P. R. China*

[b]*Shandong Provincial Key Laboratory of Preparation and Measurement of Building Materials, University of Jinan, Jinan 250022, China*

Abstract

Dependence of microwaves dielectric properties on the structural characteristics of $ZnZr(Nb_{1-x}A_x)_2O_8$ (A=Ta, Sb) ($0 \le x \le 0.10$) ceramics is investigated. All the compounds are prepared by a conventional solid-state reaction method and analyzed via multiphase structure refinement. The diffraction patterns of $ZnZr(Nb_{1-x}A_x)_2O_8$ (A=Ta, Sb) shows that the monoclinic wolframite structure of $ZrZrNb_2O_8$ which consists of an oxygen octahedral, and with the Nb ion in the center of the oxygen octahedral. For the $ZnZr(Nb_{1-x}A_x)_2O_8$ (A=Ta, Sb) ceramics, the dielectric constant (ε_r) decreased due to decrease in Nb-site bond ionicity. Quality factor ($Q \times f$) of $ZnZr(Nb_{1-x}Sb_x)_2O_8$ ceramics is found be highest (89,400GHz), which is explained in terms of average of Nb-site lattice energy. With the decreasing of bond energy of Nb-site, the temperature coefficient of resonant frequency ($|\tau_f|$) value increased. The substitution of A^{5+} (A=Ta, Sb) for Nb^{5+} effectively influences the microstructure and the microwave dielectric properties of $ZrZrNb_2O_8$ ceramics.

Keywords: Crystal structure; Substitution; Bond ionicity; Lattice energy; Bond energy; ceramics

1. Introduction

*Corresponding author. Tel. : +86 13702194791

Email address: zptai@163.com (P. Zhang)

The microwave dielectric ceramics plays an important role in the development of global positioning systems, intelligent transport systems and satellite broadcasting [1, 2]. These materials, which used in the microwave band, are very effective for making smaller devices and improving the packaging density of microwave integrated circuits. Requirements for the microwave dielectric ceramics should have high relative permittivity (ε_r>10), high quality factor ($Q\times f$>10,000 GHz) and near zero temperature coefficient of resonant frequency (τ_f=0 ppm/^{o}C) for miniaturization, better selectivity and stability, respectively [3-4]. In order to meet the specifications of current and future development, numbers researchers are focusing on exploring new excellent microwave dielectric materials.

Recently, great attention has been paid to new low dielectric loss materials of $ZnZrNb_2O_8$ with monoclinic wolframite crystal structure [5-9]. The $ZnZrNb_2O_8$ ceramics, which possessed excellent microwave dielectric properties of ε_r=30, $Q\times f$=61,000 GHz and τ_f= -52 ppm/^{o}C, were first reported by *Liao. et al* [5]. *Ramarao et al*[6]. investigated the crystal structure refinement and microwave dielectric properties of new low dielectric loss $AZrNb_2O_8$ (A: Mn, Mg, Zn and Co) and reported the dielectric properties of $ZnZrNb_2O_8$ ceramics with ε_r=16.5, $Q\times f$=53,400 GHz and τ_f= -49.8 ppm/^{o}C. Then *Cheng et al* [7]. reported dielectric properties of $MgZrNb_2O_8$ ceramics. *Tang et al* [8]. presented the effects of $BaCu(B_2O_5)$ addition on the microwave dielectric properties of $ZnZrNb_2O_8$ ceramics. An maximum $Q\times f$ values of 56,720 GHz was obtained from $ZnZrNb_2O_8$ ceramics doped with 3 wt.% $BaCu(B_2O_5)$ additions sintered at 950^{o}C for 4 h. Recently, *Li et al* [9]. have studied the difference of ions substitution on the microwave dielectric properties of $(Zn_{0.95}M_{0.05})ZrNb_2O_8$ (M=Ni, Mg, Co, Mn), with x=0.05 Ni^{2+} ions addition, the optimal $Q\times f$ values (83,558 GHz) for $ZnZrNb_2O_4$ ceramics can be obtained. However, the variation of microwave dielectric properties with substitution of different pentavalent ions on Nb-site in

$ZnZrNb_2O_8$ was not discussed. Moreover, the relationship between bond ionicity, lattice energy, bond energy and microwave dielectric properties of $ZnZr(Nb_{1-x}A_x)_2O_8$ (A=Ta, Sb) was also not investigated.

Therefore, in this paper, the correlations between microstructure and microwave dielectric properties of $ZnZr(Nb_{1-x}A_x)_2O_8$ (A=Ta, Sb) were systematically discussed. In addition, the bond ionicity, lattice energy and bond energy were calculated based on the complex chemical bond theory. An available method based on the Rietveld refinement of X-ray techniques was also used to analyze the structures of crystalline phases.

2. Experimental procedure

The ceramics were prepared through a conventional solid-state reaction route. High-purity oxide powders ZnO (99.9%), ZrO_2 (99.0%), Nb_2O_5 (99.9%), Ta_2O_5 (99.9%), and Sb_2O_5 (99.9%) were used as the starting materials. The raw materials were mixed according to the formula of $ZnZr(Nb_{1-x}A_x)_2O_8$ (A=Ta, Sb) (x=0.0, 0.02, 0.04, 0.06, 0.08, 0.1). The mixed powders were milled 6 h with distilled water in a nylon container with ZrO_2 balls. All the slurries were dried and pre-sintered at 1100 ^oC for 4 h. The pre-sintered powders were re-milled 8 h. After drying, crushed and sieved with an 80 mesh screen, the powders were pressed into disk-typepellets with 10 mm diameter and 5 mm thickness at 100 MPa. Then these pellets were sintered at temperatures of 1250^oC for 4 h in air with the heating rate of 5^oC/min.

The crystalline phases of the sintered samples were identified by X-ray diffraction (XRD, Rigaku D/max 2550 PC, Tokyo, Japan) with Cu Kα radiation generated at 40 kV and 40 mA. The microstructure of the ceramic surfaces were performed and analyzed by a scanning electron microscopy (SEM, MERLIN Compact, Germany). The microwave dielectric properties were measured in the frequency range of 6-10 GHz using a HP8720ES network analyzer [10]. The temperature coefficients of resonant frequency (τ_f)

were measured in the temperature range from 25 °C to 85 °C. The τ_f (ppm/ °C) value calculated by noting the change in resonant frequency (Δf)

$$\tau_f = \frac{f_2 - f_1}{f_1(T_2 - T_1)} \quad (1)$$

where f_1 is resonant frequency at T_1 and f_2 is the resonant frequency at T_2.

The apparent densities of the sintered pellets were measured use the Archimedes method (Mettler ToledoXS64). To study the relative density of the sample, the theoretical density was obtained from the crystal structure and atomic weight by the Eq. (2):

$$\rho_{theory} = \frac{ZA}{V_C N_A} \quad (2)$$

where V_C, N_A , Z, and A are volume of unit cell (cm^3), avogadro number (mol^{-1}), number of atoms in unit cell, and atomic weight (g/mol), respectively. The relative density was obtained by the Eq. (3):

$$\rho_{relative} = \frac{\rho_{bulk}}{\rho_{theory}} \times 100\% \quad (3)$$

3. Results and discussion

3.1Multiphase refinement

The X-ray diffraction patterns of $ZnZr(Nb_{1-x}A_x)_2O_8$ (A=Ta, Sb) ($0 \le x \le 0.10$) ceramics sintered at 1250°C for 4 h are given in Fig. 1. All parameters of interest including scale factors for all phases, zero point, background, half-width, asymmetry parameters, unit-cell parameters, atomic positional coordinates, temperature factors are refined step-by-step for avoiding correlations using the Full-Prof. All the reflections are well matched with the PDF file no. 48-0324 according to the JADE 6, and the refinement is found to belong to the monoclinic wolframite structure with the space group P2/c (no. 13). From the x values of A^{5+} (A=Ta, Sb) ionic increases, which decreases the lattice parameters. Therefore, the unit cell volume decreases and causes the reflections to shift to higher angles, which can be seen in the illustration

of the Fig.1 (a), (b) and (c). As shown in the Fig. 1(b), with the Sb^{5+} substitution increase to 0.10, we can found that abnormal peaks were appeared at the position of 002 and 130, it indicates that the solid solubility of the Sb^{5+} substitution is 0.08. Fig. 2 shows the profile fits for the Rietveld refinement of $ZnZrNb_2O_8$ ceramic. The starting model for this refinement was taken from *Macavei et al.*[11]. According to the Rietveld refinement, the lattice parameters are calculated as a=4.813 Å, b=5.674 Å, c=5.067 Å, β=91.45° and V=138.56 $Å^3$, the Rietveld discrepancy factors R_p and R_{wp} are 11.41% and 12.42%. The part of refinement results such as lattice parameters and bond length given in Table.1, Table.2 (a) and (b). From the refinement results, we can observe that with the increasing of the x values, both of the unit cell volumes for Ta^{5+} and Sb^{5+} substitutions are decreasing. The reason why the unit cell volumes for Sb^{5+} substitution have a smaller value, it could be due to that the substitution of Sb^{5+} ((ionic radius, abbr. r=0.60 Å, coordination numbers, abbr. CN = 6)) ion is smaller than the Ta^{5+} ((ionic radius, abbr. r=0.64 Å, coordination numbers, abbr. CN = 6)) ion. Therefore, the substitution of Nb^{5+} ion by Sb^{5+} could have a smaller unit cell volume.

3.2 Crystal structure analysis

The $CdWO_4$ reported by *Macavei et al.*[11] is adopted as the starting model of Rietveld refinement. Table.3 shows the refined atomic coordinate of $ZnZrNb_2O_8$ ceramics. Based on the atomic coordinate information, a schematic representation of a $ZnZrNb_2O_8$ supercell (1×1×1) is given in Fig. 3. In the supercell, there contains one $ZnZrNb_2O_8$ molecules per primitive cell and consists of an oxygen octahedron, with the Nb ion at the center of the oxygen octahedron, as shown in Fig. 3. Due to the special structure, the variation of the oxygen octahedron has vital effect on the microwave dielectric properties. In this paper, with the increase of substitution ions, the atomic interactions of $ZnZrNb_2O_8$ ceramics are

changed, which could result in bond length of the oxygen octahedron. The change of the bond length of oxygen octahedron has close connection with the bond ionicity, lattice energy and bond energy, which are an intrinsic factor that is found to be affecting the microwave dielectric properties.

3.3. Microstructure analysis

The microstructures of the sintered pellets $ZnZr(Nb_{1-x}A_x)_2O_8$ (A=Ta, Sb) ($0 \le x \le 0.10$) at 1250°C are shown in the Fig. 4. With the increase of the x values, the grain sizes have no obvious change. The grains of all the specimens are homogeneous and the surface is smooth. Moreover, the grain sizes are no significant differences, all in the range of 4-6μm, which clearly indicates well-densified compounds.

3.4. Bond ionicity, lattice energy and bond energy calculation

It is well known that the concepts of chemical bond ionicity are very important for explaining many basic properties in diverse areas [12-14]. The chemical bond ionicity could be evaluated by P-V-L theory, which was generalized to application for complex crystals by *Zhang et al* [15-16]. Based on the complex bond theory and our previous work [17-18], the complex crystals $ZnZrNb_2O_8$ could be decomposed into the sum of binary crystals as follows:

$$\begin{aligned} &ZnZrNb_2O_8 = ZnZrNb_2O(1)_4O(2)_4 \\ &= Zn_{1/3}O(1)_{2/3} + Zn_{2/3}O(2)_{4/3} + Zr_{1/3}O(1)_{2/3} + Zr_{2/3}O(2)_{4/3} + Nb_{4/3}O(1)_{8/3} + Nb_{2/3}O(2)_{4/3} \\ &= Zn_{1/3}O(1)_{2/3} + Zn_{1/3}O(2)^1_{2/3} + Zn_{1/3}O(2)^2_{2/3} + Zr_{1/3}O(1)_{2/3} + Zr_{1/3}O(2)^1_{2/3} \\ &+ Zr_{1/3}O(2)^2_{2/3} + Nb_{2/3}O(1)^1_{4/3} + Nb_{2/3}O(1)^2_{4/3} + Nb_{2/3}O(2)_{4/3} \end{aligned}$$

According to the generalized P-V-L theory, the bond ionicity can be calculated using the generalized P-V-L dielectric theory as follows [17]:

$$f_i^{\mu} = \frac{\left(C^{\mu}\right)^2}{\left(E_g^{\mu}\right)^2} \tag{4}$$

$$f_C^{\mu} = \frac{\left(E_h^{\mu}\right)^2}{\left(E_g^{\mu}\right)^2} \tag{5}$$

where f_i^{μ} was the bond ionicity and f_c^{μ} was bond covalency E_g^{μ} was the average energy gap for the type bond μ, which was composed of homopolar E_h^{μ} and heteropolar C^{μ} parts as follows:

$$(E_g^{\mu})^2 = (E_h^{\mu})^2 + (C^{\mu})^2 \tag{6}$$

where

$$(E_h^{\mu})^2 = \frac{39.74}{\left(d^{\mu}\right)^{2.48}} \tag{7}$$

For any binary crystal A_mB_n type compounds, the heteropolar C^{μ} parts can be calculated from the reference 17.

Based on the generalized P-V-L theory [18-19], the lattice energy of a single-bond crystal can be separated into ionic and covalent parts. The ionic contribution to the crystal lattice energy mainly results from electrostatic interactions and repulsive interactions of the ion pairs, and the covalent contribution arises from the overlap of electron clouds. In the following paragraphs, the lattice energy U_{cal} of a complex crystal was written as follows:

$$U_{cal} = \sum_{\mu} U_b^{\mu} \tag{8}$$

$$U_b^{\mu} = U_{bc}^{\mu} + U_{bi}^{\mu} \tag{9}$$

$$U_{bc}^{\mu} = 2100m\frac{(Z_+^{\mu})^{1.64}}{(d^{\mu})^{0.75}} f_C^{\mu} \tag{10}$$

$$U_{bi}^{\mu} = 1270\frac{(m+n)Z_+^{\mu}Z_-^{\mu}}{d^{\mu}}(1-\frac{0.4}{d^{\mu}})f_i^{\mu} \tag{11}$$

where U_{bc}^{μ} was the covalent part and U_{bi}^{μ} was the ionic part of μ bond. Z_+^{μ} and Z_-^{μ} were the valence states of cation and anion which constituted bond μ.

R. T. Sanderson [20-23] reported that the bond energy could be obtained by the chemical bond and the electronegativity. In our recent work, based on the electronegativity and bond energy theory, we have

generalized the Sanderson theory and complex theory[24-25]. The bond energy E of a complex crystal could be written as:

$$E = \sum_{\mu} E_b^{\mu} \tag{12}$$

$$E_b^{\mu} = t_c E_c^{\mu} + t_i E_i^{\mu} \tag{13}$$

where E_b^{μ} was bond energy for the type μ bond. The energy of the ionic form E_i^{μ} was the unit charge product divided by the bond length d^{μ}, adjusted to kcal/ mol by the factor 33200 when the bond length was pm.

$$E_i^{\mu} = \frac{33200}{d^{\mu}} \tag{14}$$

For any binary crystal A_mB_n type compounds, the nonpolar covalence energy E_c^{μ} parts could be calculated as following:

$$E_c^{\mu} = \frac{(r_{cA} + r_{cB})}{d^{\mu}} (E_{A-A} E_{B-B})^{1/2} \tag{15}$$

where r_{cA} and r_{cB} were the covalent radii, $E_{A\text{-}A}$ and $E_{B\text{-}B}$ were the homonuclear bond energy.

For the Eq. (13), t_c and t_i were the covalent and ionic blending coefficients, respectively. The relationship of t_c and t_i can be described by the following formula:

$$t_c + t_i = 1 \tag{16}$$

The ionic blending coefficient t_i was defined as:

$$t_i = \left| \frac{(S_A - S_B) / \Delta S_B}{2} \right| \tag{17}$$

where S_A and S_B were the electronegativities of A and B ions, in this paper, S_{Zn}=1.14, S_{Zr}=1.33, S_{Nb}=1.6 and S_O=3.44. ΔS_B was the change for complete of an electron and had the value of 3.

3.5. Microwave dielectric properties analysis

The microwave dielectric properties of $ZnZr(Nb_{1-x}A_x)_2O_8$ (A=Ta, Sb) ($0 \le x \le 0.10$) ceramics are

illustrated in Table 4. At microwave frequencies, it is believe that the dielectric constant is affecting on the dielectric polarizabilities, as well as the relative density and second phases [26]. In our experiments, ε_r is mainly dependent on the changing of the dielectric polarizabilities, due to the densified specimens from the SEM patterns in Fig.4. Moreover, there is no secondary phase in the compound.

Table.5 (a) and (b) shows the calculation of bond ionicity for $ZnZr(Nb_{1-x}A_x)_2O_8$ (A=Ta, Sb) ($0 \le x \le 0.10$) ceramics. According to the calculated results, the bond ionicity of *Nb-O* bond has a higher value compared with the bond type of Zn-O and Zr-O. It is clarified that the Nb-site bond ionicity has more contribution to the bond ionicity, and the bond ionicity of Nb-O type has dominant effect on the microwave dielectric properties of $ZnZr(Nb_{1-x}A_x)_2O_8$ (A=Ta, Sb) ceramics. According to the P-V-L theory studied by *Batsanov et al* [27], the relationship between constant and bond ionicity was founded as follows:

$$\varepsilon_r = \frac{n^2 - 1}{1 - f_i} + 1 \tag{18}$$

where *n* is the refractive index. It is suggested that the dielectric constant decreased with the bond ionicity decreasing. The ε_r value and the average of Nb-site bond ionicity $Af_{iNb\text{-}O}$ for $ZnZr(Nb_{1-x}A_x)_2O_8$ (A=Ta, Sb) ($0 \le x \le 0.1$) ceramics are given in Fig.5. As Fig.5 shows, the ε_r values keep the same change trend with the average of bond ionicity $Af_{iNb\text{-}O}$ in the range of x=0-0.10. With the decreasing of the $Af_{iNb\text{-}O}$, the ε_r values keeps decreasing.

Usually, the Q×f values are controlled by many factors, and it can be divided into two fields, the intrinsic loss and extrinsic loss. The intrinsic losses are mainly caused by lattice vibration modes, while the extrinsic losses are dominated by such as second phases, oxygen vacancies, grain boundaries, and densification or porosity [28-31]. However, in this study, the effect of extrinsic loss is minimal due to the

densified compounds. In our recent work, we reported that Q×*f* values of $NdNbO_4$ ceramics were closely related to the lattice energy of the structure [17, 24, 25]. With an increase in the lattice energy, the Q×*f* values would increase. In this work, the $ZnZrNb_2O_8$ ceramics have the same structure with the $NdNbO_4$ ceramics. Therefore, the Q×*f* values of $ZnZrNb_2O_8$ ceramics were also closely dependent on the lattice energy. According the Rietveld refinement results, the calculations of lattice energy for $ZnZr(Nb_{1-x}A_x)_2O_8$ (A=Ta, Sb) ($0\leq x\leq 0.10$) ceramics shown in Table.6 (a) and (b). Fig.6 shows the Q×*f* value and the average of Nb-site lattice energy $AU_{Nb\text{-}o}$ for $ZnZr(Nb_{1-x}A_x)_2O_8$ (A=Ta, Sb) ($0\leq x\leq 0.1$) ceramics. With the substitution ions increasing, both the Q×*f* values of Ta^{5+} and Sb^{5+} substitution have an increasing trend. When x =0.10, the second phase was formed from the Fig. 1(b). Therefore, with the increase of Sb^{5+} substitution, although the Nb-site lattice energy keeps increasing, the Q×f values decreased.

Reaney et al[32]. reported that the structural characteristics of [BO6] oxygen octahedral has a closely relation with the temperature coefficient of resonant frequency τ_f values, and τ_f values will change with the variations of the bond length of oxygen octahedral. In our previous research, we have investigated that the bond energy and bond length between the octahedral-site cation and oxygen will affect the τ_f values [24, 25]. The τ_f values decreased as the bond energy of oxygen octahedral increased, and the system will tend to stable. According to the calculation results of bond energy from Table.7 (a) and (b), we can find the fact that the substitution ions have more effect on the bond energy of oxygen octahedral, with the increasing of the substitution values, the average of Nb-site bond energy decreased. Fig.7 gives the τ_f value and the average of Nb-site bond energy $AE_{Nb\text{-}o}$ for $ZnZr(Nb_{1-x}A_x)_2O_8$ (A=Ta, Sb) ($0\leq x\leq 0.1$) ceramics. As the $AE_{Nb\text{-}o}$ decreased, the τ_f values shift to the negative direction, it indicates that the system tend to instable. The bond energy of the $ZnZr(Nb_{1-x}Sb_x)_2O_8$ have a bigger value than the bond energy of the

$ZnZr(Nb_{1-x}Ta_x)_2O_8$, which indicates the $ZnZr(Nb_{1-x}Sb_x)_2O_8$ system would be more stable and have a small $|\tau_f|$value.

4. Conclusions

The multiphase refinement was used to analysis the crystal structure of $ZnZrNb_2O_8$ ceramics. The bond ionicity, lattice energy and bond energy were calculated from Rietveld refinement results. The effects of Ta^{5+} and Sb^{5+} substitution on the microstructures and microwave dielectric properties of $ZnZrNb_2O_8$ ceramics were discussed. The ε_r was observed to decreased from 26.70 to 25.73 for Ta^{5+} substitution and 26.70 to 26.03 for Sb^{5+} substitution due to decrease in Nb-site bond ionicity. The Q×f values have a close relationship with the Nb-site lattice energy. Lower bond energy correlated with instable system, and instable system suggested that there would have a bigger $|\tau_f|$value.

Acknowledgments

The authors gratefully acknowledged supports from the Key Laboratory of Advanced Ceramics and Machining Technology, Ministry of Education (Tianjin University). In addition, this work was supported by the project of development plan of science and technology of Ji'nan City (No.201303061), Ji'nan City Youth Science and Technology Star Project (No.2013035), and National Natural Science Foundation (No. 51472108).

References

1 L. C. Tien, C. C. Chou, D. S. Tsai, J. Am. Ceram. Soc. 83 (2000) 2074.

2 D. W. Kim, D. Y. Kim, K. S. Hong, J. Mater. Res. 15 (2000) 1331.

3 D. W. Kim, D. K. Kwon, S. H. Yoon, K. S. Hong, J. Am. Ceram. Soc. 89 (2006) 3861.

4 P. Zhang, Y. G. Zhao, J. Liu, Z. K. Song, M. Xiao, Y. X. Wang, Dalton. Trans. 44 (2015) 5053.

5 Q.W. Liao, L.X. Li, J. Am. Ceram. Soc. 95(2012) 3363.

6 S.D. Ramarao, V. R. K. Murthy, Scripta. Mater. 69 (2013) 274.

7 Y. Cheng, R.Z. Zuo, Y. Lv, Ceram. Int. 39 (2013) 8681.

8 X. Tang, H. Yang, Q. L. Zhang, J. H. Zhou, Ceram. Int. 40 (2014) 12875.

9 L. X. Li, H. Sun, H. C. Cai, X. S. Lv J. Alloy. Compd. 639 (2015) 516.

10 W. E. Courtney. IEEE Trans Microwave Theory Tech. 18 (1970) 476.

11 J. Macavei, H. Schulz, Z. Krist-Cryst. Mater. 207(1993) 193.

12 D. F Xue, S. Y. Zhang, J. Phys. Cond. Mat. 8 (1996) 1949.

13 R. D. Shannon, Acta. Cryst. A32 (1976) 751.

14 A. F. Kapustinskii, Rev. Chem. Soc. 10 (1956) 283.

15 Z. J. Wu, Q. B. Meng, S. Y. Zhang, Phy.s Rev. B. 58 (1998) 958.

16 Q. B. Meng, Z. J. Wu, S. Y. Zhang, J. Phys. Cond. Mat. 10 (1998) 85.

17 P. Zhang, Y. G. Zhao, Y. X. Wang, Dalton. Trans. 44 (2015) 10932.

18 D. T. Liu, S. Y. Zhang, Z. J. Wu, Inorg. Chem. 42 (2003) 2465.

19 W. S. Xia, L. X. Li, P. F. Ning, Q. W. Liao, J. Am. Ceram. Soc. 95 (2012) 1.

20 R. T. Sandderson, Inorg. Nucl. Chem. 28 (1966) 1553.

21 R. T. Sandderson, Inorg. Nucl. Chem.30 (1968) 375.

22 R. T. Sandderson, Chemical Bonds and Bond Energy. Academic Press: New York 1971.

23 R. T. Sandderson, J. Am. Chem. Soc. 105 (1983) 2259.

24 P. Zhang, Y. G. Zhao, X. Y. Wang, J. Alloy. Compd. 644 (2015) 621.

25 P. Zhang, Y. G. Zhao, X. Y. Wang, J. Alloy. Compd. 647 (2015) 386.

26 P. Zhang, Z. K. Song, Y. Wang, L.X. Li, J. Am. Ceram. Soc. 97 (2014) 976.

27 S. S. Batsanov, Russ. Chem. Rev. 51(1982) 684.

28 Q. W. Liao, L. X. Li, Dalton. Trans. 41(2012) 6963.

29 D. Zhou , Li X. Pang, H. Wang, X. Yao, Solid. State. Sci. 11 (2009) 1894.

30 R. D. Shannon, J. Appl. Phys. 73 (1993) 348.

31 C, L, Huang, S, S, Liu, J. Appl. Phys. 46 (2007) 283.

32 I. M. Reaney, E. L. Colla, and N. Setter, Jpn. Appl. Phys. 33 (1994) 3984.

A table of contents entry

Bond iconicity, lattice energy and bond energy were calculated from the Rietveld refinement.

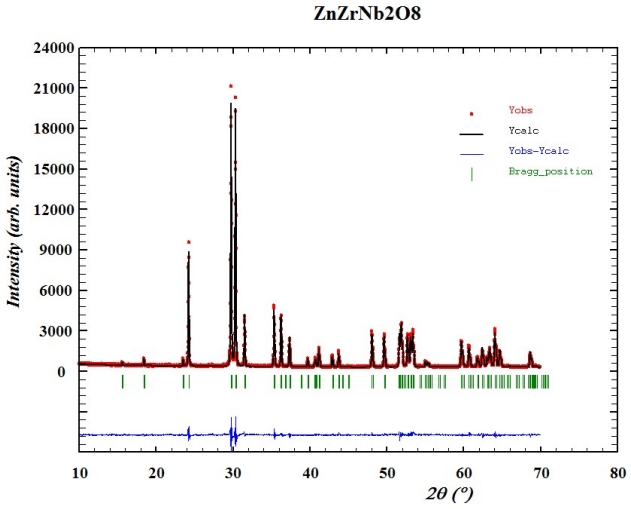

Figure captions

Fig.1 (a) The XRD patterns of $ZnZr(Nb_{1-x}Ta_x)_2O_8$ ($0.02\leq x\leq 0.10$) ceramics sintered at 1250 °C for 4h; (b) The XRD patterns of $ZnZr(Nb_{1-x}Sb_x)_2O_8$ ($0.02\leq x\leq 0.10$) ceramics sintered at 1250 °C for 4h; (c) The XRD patterns of $ZnZrNb_2O_8$, $ZnZr(Nb_{0.92}Ta_{0.08})_2O_8$, and $ZnZr(Nb_{0.92}Sb_{0.08})_2O_8$ ceramics sintered at 1250 °C for 4h.

Fig.2 The profile fits for the Rietveld refinement of $ZnZrNb_2O_8$ ceramic.

Fig.3 The crystal structure patterns (1 × 1 × 1) supercell of monoclinic wolframite structured $ZnZrNb_2O_8$.

Fig.4 The SEM photographs of $ZnZr(Nb_{1-x}A_x)_2O_8$ (A=Ta, Sb) ($0\leq x\leq 0.1$) ceramics.

Fig.5 The ε_r value and the average of Nb-site bond ionicity $Af_{iNb\text{-}O}$ for $ZnZr(Nb_{1-x}A_x)_2O_8$ (A=Ta, Sb) ($0\leq x\leq 0.1$) ceramics.

Fig.6 The $Q\times f$ value and the average of Nb-site lattice energy $AU_{Nb\text{-}o}$ for $ZnZr(Nb_{1-x}A_x)_2O_8$ (A=Ta, Sb) ($0\leq x\leq 0.1$) ceramics.

Fig.7 The τ_f value and the average of Nb-site bond energy $AE_{Nb\text{-}o}$ for $ZnZr(Nb_{1-x}A_x)_2O_8$ (A=Ta, Sb) ($0\leq x\leq 0.1$) ceramics.

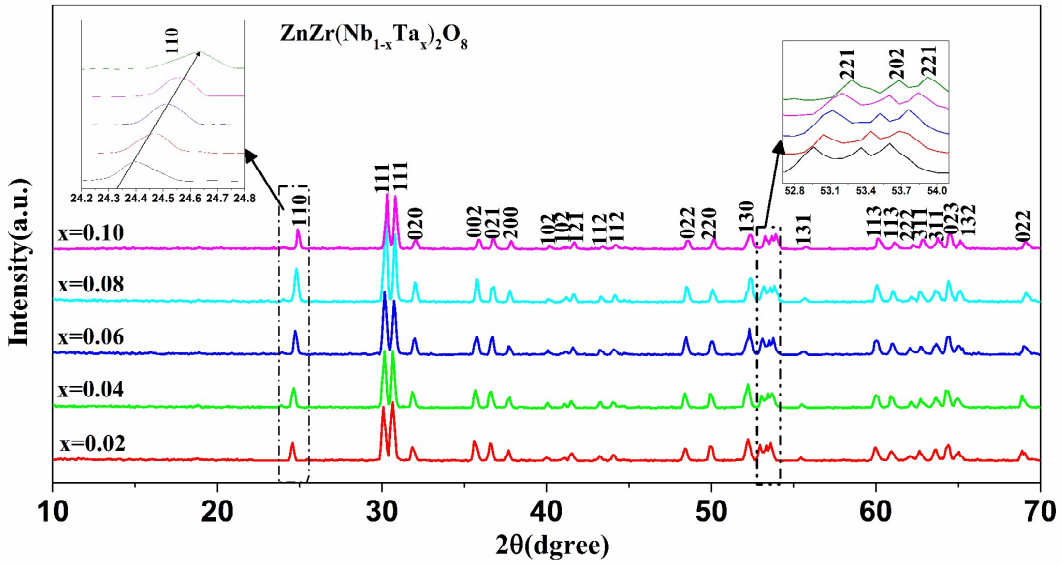

Fig.1 (a)

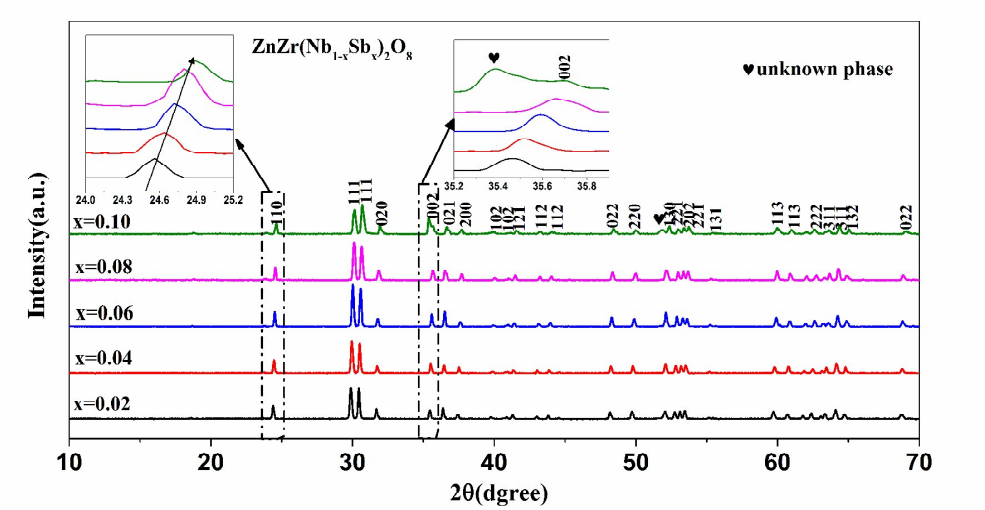

Fig.1 (b)

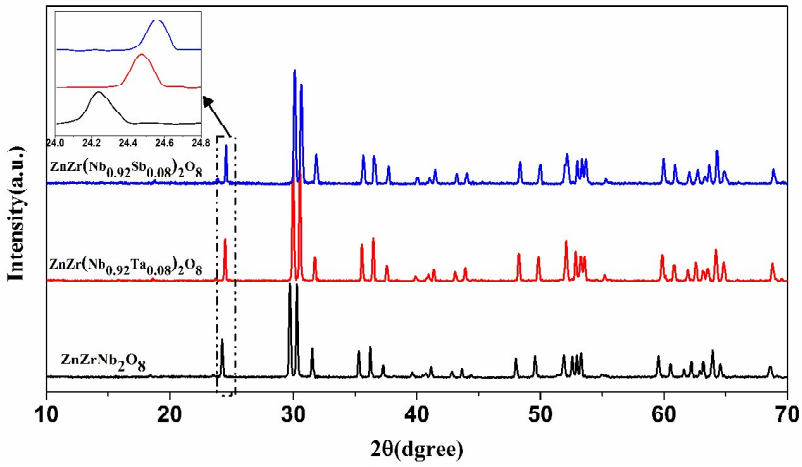

Fig.1 (b)

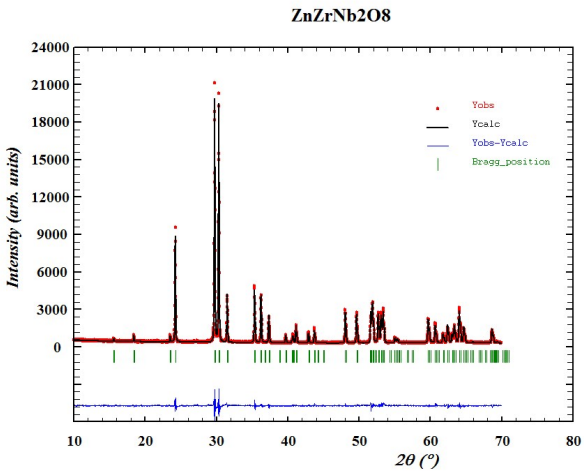

Fig.2

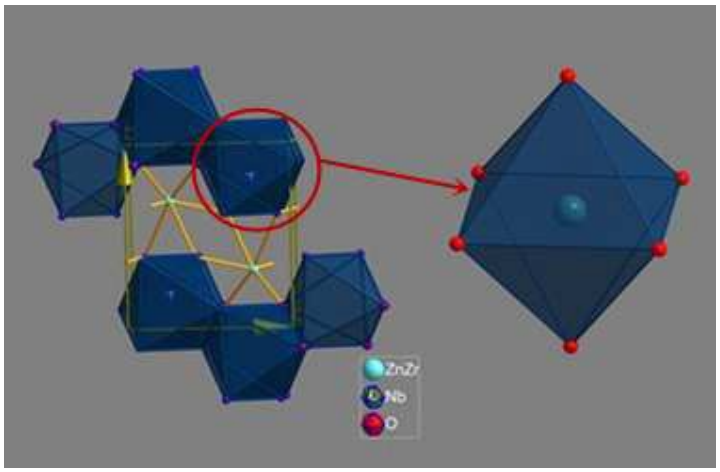

Fig.3

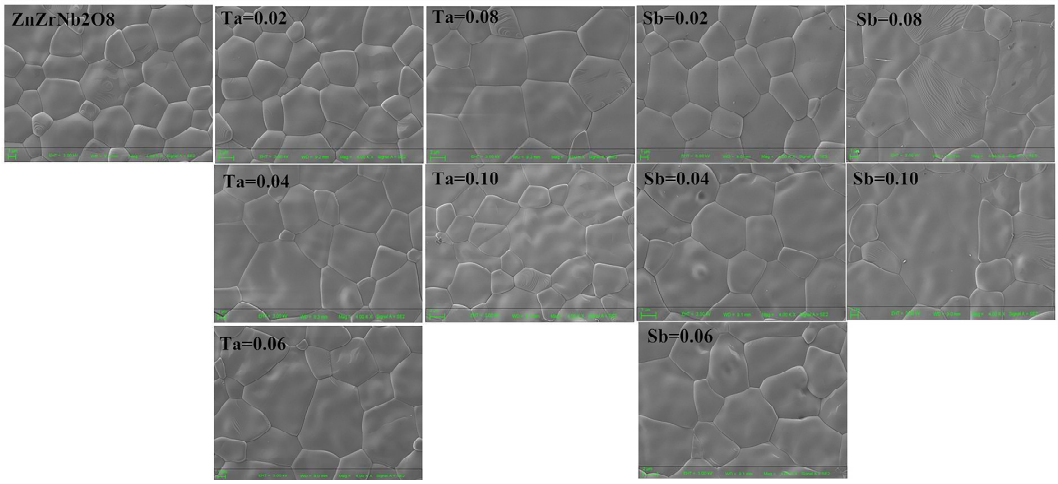

Fig. 4

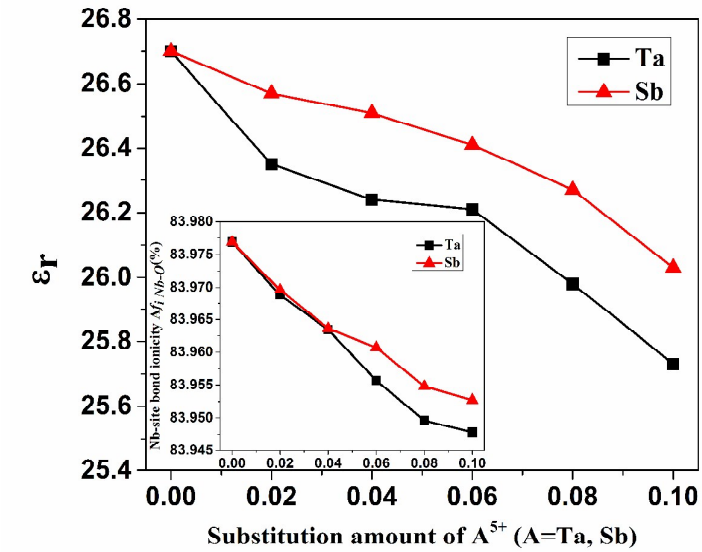

Fig.5

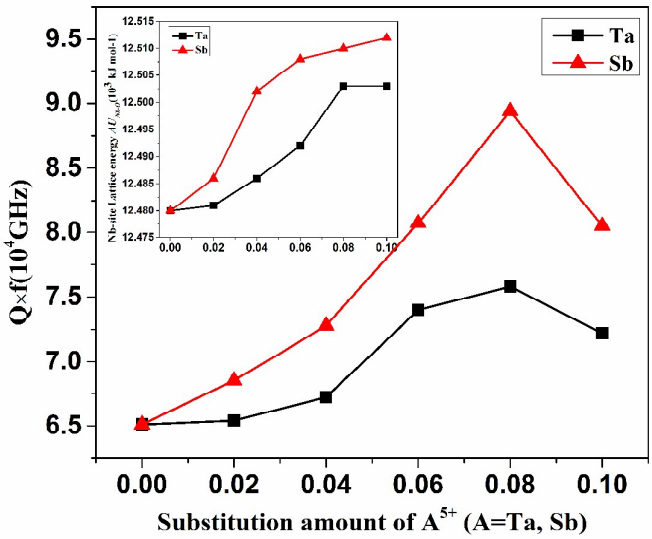

Fig.6

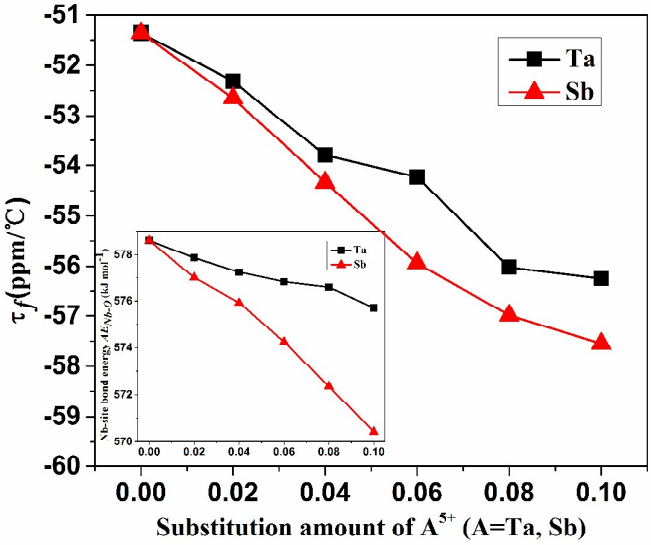

Fig.7

Table.1 Crystallographic data from Rietveld refinement for $ZnZr(Nb_{1-x}A_x)_2O_8$ (A=Ta, Sb) (0≤x≤0.10) ceramics

Type	*a (Å)*	*b(Å)*	*c(Å)*	*β(°)*	*V(Å^3)*	*R_p(%)*	*R_{wp}(%)*
$ZnZrNb_2O_8$	4.813	5.674	5.076	91.45	138.56	11.41	12.42
$ZnZr(Nb_{1-x}Ta_x)_2O_8$							
x=0.02	4.793	5.706	5.063	90.96	138.44	9.29	14.90
x=0.04	4.770	5.688	5.092	90.27	138.15	9.46	13.67
x=0.06	4.757	5.716	5.072	90.57	137.91	8.67	14.87
x=0.08	4.754	5.715	5.061	90.92	137.49	9.12	14.46
x=0.10	4.739	5.678	5.105	90.20	137.35	7.69	10.36
$ZnZr(Nb_{1-x}Sb_x)_2O_8$							
x=0.02	4.810	5.690	5.050	90.68	138.20	10.27	13.60
x=0.04	4.798	5.662	5.067	91.48	137.61	9.06	11.15
x=0.06	4.796	5.655	5.065	91.39	137.33	9.98	10.74
x=0.08	4.777	5.665	5.069	90.83	137.16	8.73	11.73
x=0.10	4.775	5.662	5.069	90.48	137.04	7.64	13.84

Table.2 (a) Bond length (*Å*) for $ZnZr(Nb_{1-x}Ta_x)_2O_8$ (0≤x≤0.10) ceramics

Type	x=0	Ta(0.02)	Ta(0.04)	Ta(0.06)	Ta(0.08)	Ta(0.10)
Zn-O(1)×2	2.0195	2.0130	2.0018	2.0042	2.0064	1.9954
Zn-O(2)^1×2	2.0852	2.0877	2.1038	2.0922	2.0831	2.1046
Zn-O(2)^2×2	2.2177	2.2186	2.2084	2.2144	2.2156	2.2026
Ti-O(1)×2	2.0195	2.0130	2.0018	2.0042	2.0064	1.9954

Ti-O(2)^1×2	2.0852	2.0877	2.1038	2.0922	2.0831	2.1046
Ti-O(2)^2×2	2.2177	2.2186	2.2084	2.2144	2.2156	2.2026
Nb-O(1)^1×2	1.9815	1.9688	1.9626	1.9609	1.9630	1.9608
Nb-O(1)^2×2	2.1825	2.1905	2.1921	2.1927	2.1885	2.1882
Nb-O(2)×2	1.8858	1.8902	1.8923	1.8893	1.8846	1.8871

Table.2 (b) Bond length (*Å*) for $ZnZr(Nb_{1-x}Sb_x)_2O_8$ ($0.02\leq x\leq 0.10$) ceramics

Type	Sb(0.02)	Sb(0.04)	Sb(0.06)	Sb(0.08)	Sb(0.010)
Zn-O(1)×2	2.0100	2.0149	2.0125	2.0044	1.9999
Zn-O(2)^1×2	2.0904	2.0803	2.0808	2.0889	2.0942
Zn-O(2)^2×2	2.2141	2.2128	2.2101	2.2064	2.2030
Ti-O(1)×2	2.0100	2.0149	2.0125	2.0044	1.9999
Ti-O(2)^1×2	2.0904	2.0803	2.0808	2.0889	2.0942
Ti-O(2)^2×2	2.2141	2.2128	2.2101	2.2064	2.2030
Nb-O(1)^1×2	1.9632	1.9775	1.9753	1.9657	1.9601
Nb-O(1)^2×2	2.1901	2.1774	2.1762	2.1813	2.1833
Nb-O(2)×2	1.8930	1.8809	1.8804	1.8839	1.8865

Table.3 The refined atomic coordinate of $ZnZrNb_2O_8$ ceramic.

Element	Wyckoff site	x	y	z	OCC
Zn	2f	0.50000	0.68856	0.25000	0.5
Zr	2f	0.50000	0.68856	0.25000	0.5
Nb	2e	0.00000	0.18317	0.25000	1.0
O1	4g	0.22452	0.10786	0.93916	1.0

O2	4g	0.26568	0.38588	0.40895	1.0

Table.4 The microwave dielectric properties of $ZnZr(Nb_{1-x}A_x)_2O_8$ (A=Ta, Sb) (0≤x≤0.10) ceramics

Type	ε_r	$Q\times f$ (10^4 GHz)	τ_f (ppm/°C)
$ZnZrNb_2O_8$	26.70	6.51	-51.36
$ZnZr(Nb_{1-x}Ta_x)_2O_8$			
x=0.02	26.35	6.54	-52.31
x=0.04	26.24	6.72	-53.80
x=0.06	26.21	7.40	-54.23
x=0.08	25.98	7.58	-56.02
x=0.10	25.73	7.22	-56.25
$ZnZr(Nb_{1-x}Sb_x)_2O_8$			
x=0.02	26.57	6.85	-52.65
x=0.04	26.51	7.28	-54.34
x=0.06	26.41	8.07	-55.94
x=0.08	26.27	8.94	-56.99
x=0.10	26.03	8.05	-57.55

Table.5 (a) Bond ionicity for $ZnZr(Nb_{1-x}Ta_x)_2O_8$ (0≤x≤0.10) ceramics

Bond type	**Bond Ionicity f_i (%)**					
	x=0	*x=0.02*	*x=0.04*	*x=0.06*	*x=0.08*	*x=0.10*
Zn-O(1)×2	63.3780	63.3116	63.2064	63.2242	63.2442	63.1402
Zn-O(2)[1]×2	63.9399	63.9521	64.0784	63.9809	63.9066	63.0772
Zn-O(2)[2]×2	64.9372	64.9349	64.8604	64.8980	64.9063	64.8121

Ti-O(1)×2	80.2169	80.1845	80.1358	80.1426	80.1517	80.1035
Ti-O(2)^1×2	80.4642	80.4667	80.5196	80.4764	80.4444	80.5165
Ti-O(2)^2×2	80.8777	80.8737	80.8428	80.8562	80.8595	80.8206
Nb/Ta-O(1)^1×2	83.9203	83.8762	83.8545	83.8465	83.8531	83.8428
Nb/Ta-O(1)^2×2	84.4072	84.4166	84.4170	84.4153	84.4075	84.4045
Nb/Ta-O(2)×2	83.6032	83.6137	83.6188	83.6053	83.5882	83.5950
A $f_{i\ Nb\text{-}O}$ *	83.9769	83.9688	83.9634	83.9557	83.9496	83.9478

***The *A $f_{i\ Nb\text{-}O}$* was the average of the Nb/Ta-O bond ionicity.**

Table.5 (b) Bond ionicity for $ZnZr(Nb_{1-x}Sb_x)_2O_8$ ($0 \le x \le 0.10$) ceramics

Bond type	**Bond Ionicity *f_i (%)***					
	x=0	***x=0.02***	***x=0.04***	***x=0.06***	***x=0.08***	***x=0.10***
Zn-O(1)×2	63.3780	63.2896	63.3368	63.3163	63.2376	63.1955
Zn-O(2)^1×2	63.9399	63.9792	63.8996	63.9047	63.9658	64.0077
Zn-O(2)^2×2	64.9372	64.9091	64.9033	64.8855	64.8542	64.8293
Ti-O(1)×2	80.2169	80.1762	80.1984	80.1895	80.1523	80.1329
Ti-O(2)^1×2	80.4642	80.4801	80.4468	80.4493	80.4739	80.4916
Ti-O(2)^2×2	80.8777	80.8654	80.8643	80.8576	80.8431	80.8327
Nb/Sb-O(1)^1×2	83.9203	83.8623	83.9082	83.9022	83.8692	83.8510
Nb/Sb-O(1)^2×2	84.4072	84.4193	84.3974	84.3958	84.4019	84.4049
Nb/Sb-O(2)×2	83.6032	83.6272	83.5852	83.5841	83.5934	83.6021
A $f_{i\ Nb\text{-}O}$ *	83.9769	83.9696	83.9636	83.9607	83.9548	83.9527

***The *A $f_{i\ Nb\text{-}O}$* was the average of the Nb/Sb-O bond ionicity.**

Table.6 (a) Lattice energy for $ZnZr(Nb_{1-x}Ta_x)_2O_8$ ($0 \le x \le 0.10$) ceramics

Bond type	Lattice energy *U (eV)*					
	x=0	*x=0.02*	*x=0.04*	*x=0.06*	*x=0.08*	*x=0.10*
Zn-O(1)×2	1111	1114	1119	1117	1117	1122
Zn-O(2)^1×2	1082	1082	1076	1080	1084	1075
Zn-O(2)^2×2	1031	1030	1034	1032	1032	1037
Ti-O(1)×2	4030	4040	4058	4054	4051	4067
Ti-O(2)^1×2	3934	3931	3907	3924	3937	3906
Ti-O(2)^2×2	3752	3751	3765	3757	3756	3772
Nb/Ta-O(1)^1×2	12620	12680	12710	12718	12708	12719
Nb/Ta-O(1)^2×2	11732	11698	11692	11689	11706	11708
Nb/Ta-O(2)×2	13088	13066	13055	13070	13094	13081
AU $_{Nb-O}$ *	12480	12481	12486	12492	12503	12503

***The AU_{Nb-O} was the average of the Nb/Ta-O lattice energy.**

Table.6 (b) Lattice energy for $ZnZr(Nb_{1-x}Sb_x)_2O_8$ ($0 \le x \le 0.10$) ceramics

Bond type	Lattice energy *U (eV)*					
	x=0	*x=0.02*	*x=0.04*	*x=0.06*	*x=0.08*	*x=0.10*
Zn-O(1)×2	1111	1115	1113	1114	1117	1119
Zn-O(2)^1×2	1082	1081	1085	1085	1081	1079
Zn-O(2)^2×2	1031	1032	1032	1034	1035	1036
Ti-O(1)×2	4030	4044	4037	4041	4053	4060
Ti-O(2)^1×2	3934	3926	3941	3940	3929	3921
Ti-O(2)^2×2	3752	3757	3759	3762	3768	3772

Nb/Sb-O(1)^1×2	12620	12707	12639	12649	12695	12723
Nb/Sb-O(1)^2×2	11732	11700	11753	11758	11736	11729
Nb/Sb-O(2)×2	13088	13051	13113	13116	13098	13084
A U_{Nb-O} *	12480	12486	12502	12508	12510	12512

***The AU_{Nb-O} was the average of the Nb/Sb-O lattice energy.**

Table.7 (a) Bond energy for $ZnZr(Nb_{1-x}Ta_x)_2O_8$ (0≤x≤0.10) ceramics

Bond type	**Bond energy *E* (kJ/mol)**					
	x=0	***x=0.02***	***x=0.04***	***x=0.06***	***x=0.08***	***x=0.10***
Zn-O(1)×2	271.25	272.13	273.65	273.33	273.03	274.53
Zn-O(2)^1×2	262.71	262.39	260.39	261.83	262.97	260.29
Zn-O(2)^2×2	247.01	246.91	248.05	247.38	247.25	248.71
Ti-O(1)×2	510.33	511.98	514.85	514.23	513.66	516.50
Ti-O(2)^1×2	494.25	493.66	489.88	492.60	494.75	489.70
Ti-O(2)^2×2	464.72	464.53	466.68	465.42	465.16	467.91
Nb/Ta-O(1)^1×2	586.69	589.59	590.56	590.18	588.65	588.42
Nb/Ta-O(1)^2×2	532.66	529.91	528.73	527.79	528.00	527.27
Nb/Ta-O(2)×2	616.46	614.10	612.50	612.54	613.14	611.40
A E_{Nb-O} *	578.60	577.87	577.26	576.84	576.60	575.70

***The *A* E_{Nb-O} was the average of the Nb/Ta-O bond energy.**

Table.7 (b) Bond energy for $ZnZr(Nb_{1-x}Sb_x)_2O_8$ (0≤x≤0.10) ceramics

Bond type	**Bond energy *E* (kJ/mol)**					
	x=0	***x=0.02***	***x=0.04***	***x=0.06***	***x=0.08***	***x=0.10***
Zn-O(1)×2	271.25	272.54	271.87	272.20	273.30	273.91

Zn-O(2)^1×2	262.71	262.05	263.33	263.26	262.24	261.58
Zn-O(2)^2×2	247.01	247.41	247.56	247.86	248.28	248.66
Ti-O(1)×2	510.33	512.74	511.50	512.11	514.18	515.33
Ti-O(2)^1×2	494.25	493.02	495.42	495.30	493.38	492.13
Ti-O(2)^2×2	464.72	465.48	465.75	466.32	467.10	467.82
Nb/Sb-O(1)^1×2	586.69	590.10	583.79	582.38	583.13	582.69
Nb/Sb-O(1)^2×2	532.66	528.97	530.19	528.61	525.50	523.13
Nb/Sb-O(2)×2	616.46	611.99	613.77	611.77	608.45	605.43
A E_{Nb-O} *	578.60	577.02	575.92	574.25	572.36	570.42

***The *A E_{Nb-O}* was the average of the Nb/Sb-O bond energy.**